

Stable growth mechanisms of ice disk crystals in heavy water

Satoshi Adachi,^{1,*} Izumi Yoshizaki,¹ Takehiko Ishikawa,¹ Etsuro Yokoyama,² Yoshinori Furukawa,³ and Taro Shimaoka⁴

¹*Institute of Space and Astronautical Science, Japan Aerospace Exploration Agency, 2-1-1 Sengen, Tsukuba-shi, Ibaraki-ken 305-8505, Japan*

²*Computer Centre, Gakushuin University, 1-5-1 Mejiro, Toshima-ku, Tokyo 171-8588, Japan*

³*Institute of Low Temperature Science, Hokkaido University, Kita-19, Nishi-8, Kita-ku, Sapporo 060-0819, Japan*

⁴*Japan Space Forum, Shin-Ochanomizu Urban Trinity Bldg. 2F, 3-2-1 Kandasurugadai, Chiyoda-ku, Tokyo 101-0062, Japan*

(Received 8 July 2011; revised manuscript received 28 October 2011; published 22 November 2011)

Ice crystal growth experiments in heavy water were carried out under microgravity to investigate the morphological transition from a disk crystal to a dendrite. Surprisingly, however, no transition was observed, namely, the disk crystal or dendrite maintained its shape throughout the experiments, unlike the results obtained on the ground. Therefore, we introduce a growth model to understand disk growth. The Gibbs-Thomson effect is taken into account as a stabilization mechanism. The model is numerically solved by varying both an interfacial tension of the prism plane and supercooling so that the final sizes of the crystals can become almost the same to determine the interfacial tension. The results are compared with the typical experimental ones and thus the interfacial tension is estimated to be 20 mJ/m². Next, the model is solved under two supercooling conditions by using the estimated interfacial tension to understand stable growth. Comparisons between the numerical and experimental results show that our model explains well the microgravity experiments. It is also found that the experimental setup has the capability of controlling temperature on the order of 1/100 K.

DOI: [10.1103/PhysRevE.84.051605](https://doi.org/10.1103/PhysRevE.84.051605)

PACS number(s): 81.10.Aj, 81.10.Fq, 81.10.Mx

I. INTRODUCTION

A disk or hexagonal prism shape of an ice crystal in water is well known as a stable morphology. Under certain supercooling conditions, however, the stable crystal becomes morphologically unstable. First, one side of the crystal edges begins to undulate azimuthally. Then, the undulations grow like cellular growth and finally change to dendrites. This process has been investigated both experimentally [1–4] and theoretically [5–8] for a long time. The trigger of the instability, however, is not clear yet. As a first approach, the Mullins-Sekerka theory was applied to the azimuthal undulations but did not agree well with the experimental results. Next, a hypothesis of the critical thickness was proposed [3,9,10]. This hypothesis is that the crystal becomes unstable if the crystal thickness is larger than a certain threshold value. To verify this, thermal convection must be sufficiently suppressed since the convection causes temperature nonuniformity. Therefore, we planned to carry out microgravity experiments since 1993 because microgravity suppresses the buoyancy-driven convection [11].

From December 2008 to February 2009, we performed microgravity experiments of ice crystal growth in heavy water with the Japanese Experiment Module “Kibo” on the International Space Station (ISS) [12,13]. Data from more than 130 experiments were successfully obtained. Against our initial expectation, however, we were unable to observe the morphological transition from the stable disk crystal to dendrites. Namely, the stable shape was maintained over the experimental period, while the unstable shape was observed from the initial stage. This means that unfortunately one of the initial objectives of the microgravity experiment for verification of the hypothesis was not achieved but another important issue appeared, that is, why the transition did not occur.

Figure 1 shows the typical observation result under microgravity. Figure 1(a) is a snapshot of the stable growth at a supercooling setting of 0.04 K and Fig. 1(b) shows that of the unstable growth at a setting of 0.06 K. In this paper, supercooling is defined as the difference the setting temperature of the bulk heavy water from the melting point (3.82 °C), that is, $\Delta T = T_m - T$. Positive supercooling means a lower temperature than the melting point. These supercoolings are not actual supercoolings but set values. Therefore, we use ΔT_{set} to indicate this and use ΔT_{sim} for the simulation parameter described below. In microgravity experiments, stable growth was achieved under conditions of $\Delta T_{\text{set}} \leq 0.04$ K, while unstable growth was observed under conditions of $\Delta T_{\text{set}} \geq 0.06$ K. In this paper, data with almost the same thickness of about 250 μm were used in order to compare the experimental and simulation data precisely. Although some of the crystals observed at $\Delta T_{\text{set}} = 0.05$ K seemed stable, their thickness was less than that under lower supercooling conditions. Hence, the data at $\Delta T_{\text{set}} = 0.05$ K were not used in this paper.

The experimental data on the ground are quite different from those under microgravity, that is, the morphological transition from the disk shape to dendrites is often observed on the ground in a wide supercooling range as shown in Fig. 2. Figures 2(a) and 2(b) show the typical results of stable and unstable growth in a low supercooling setting of 0.02 K, respectively, while Figs. 2(c) and 2(d) show those in a large setting of 0.43 K, respectively. All data were obtained by using an engineering model of an apparatus for the microgravity experiment, which is basically the same apparatus as the flight model described in the next section. From comparison between the data under microgravity and those on the ground, it is suggested that the morphological transition may be strongly affected by thermal convection.

Therefore, we introduced a model describing the stable growth to investigate the reasons why such a difference occurs. The Gibbs-Thomson effect was taken into account

*adachi.satoshi@jaxa.jp

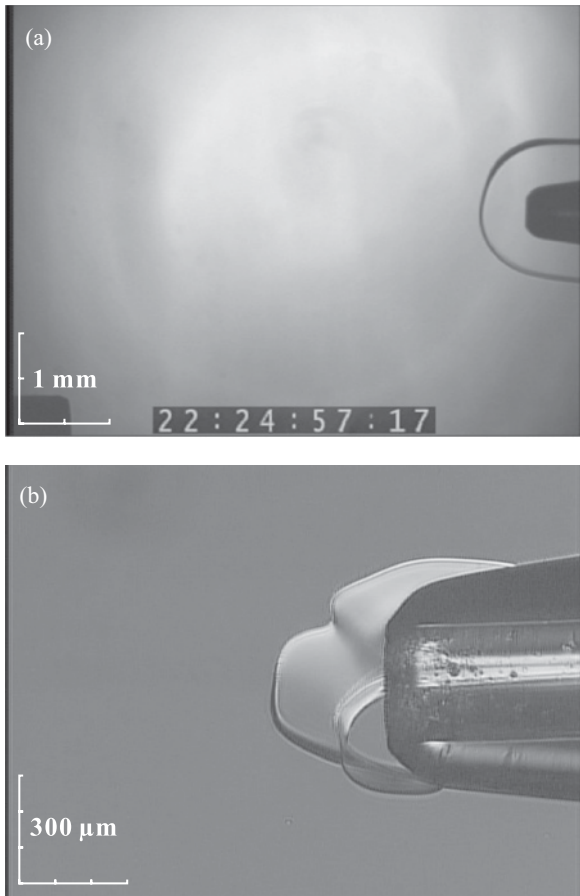


FIG. 1. Typical results of microgravity experiments of ice crystal growth: (a) $\Delta T = 0.04$ K and (b) $\Delta T = 0.06$ K. These supercoolings are set values. The former and latter results show stable and unstable growth, respectively. The difference of supercooling between the two cases is only 0.02 K.

as the stabilization mechanism since stable growth is almost impossible in the absence of stabilization mechanisms. Although the Gibbs-Thomson effect requires an interfacial

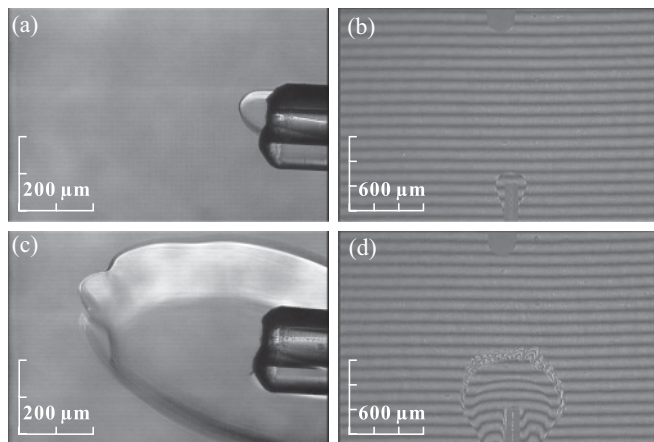


FIG. 2. Typical results of ground-based experiments of ice crystal growth: (a) stable growth in $\Delta T = 0.02$ K setting, (b) unstable growth after transition in the same setting as (a), (c) stable growth in $\Delta T = 0.43$ K setting, and (d) unstable growth after transition in the same setting as (c).

energy, the value was reported as ranging widely from 15 to 33 mJ/m² [6,14,15]. Therefore, the interfacial tension was estimated in this paper by comparing numerical data with experimental ones in the case of the $\Delta T_{\text{set}} = 0.03$ K setting. By using the estimated value, the model was solved for another comparison with $\Delta T_{\text{set}} = 0.04$ K. From these comparisons, we discuss the stabilization mechanisms, estimation of the actual supercooling in microgravity experiments, and the supercooling limit for stable growth.

II. EXPERIMENTAL SETUP

The “Kibo” module includes several facilities for microgravity experiments. In this experiment, we used the Solution Crystallization Observation Facility (SCOF). An ice crystal cell (ICC), which contains the small module shown in Fig. 3, is set on a cold plate inside the SCOF. This module is called the ice cell module (ICM) in this paper. The ICM mainly has two components, namely, the nucleation cell and the growth cell, between which a small capillary tube with an inner diameter of about 300 μm is connected. The growth cell has dimensions of 26 mm in diameter and 24 mm in height. Each cell is filled with heavy water, since the temperature dependency of its refractive index is relatively higher than that of light water, in order to detect temperature variation by interferometers more precisely.

Data shown in Fig. 1 were obtained by a bright field microscope with a field of view of 6.4 × 4.8 mm in (a), which

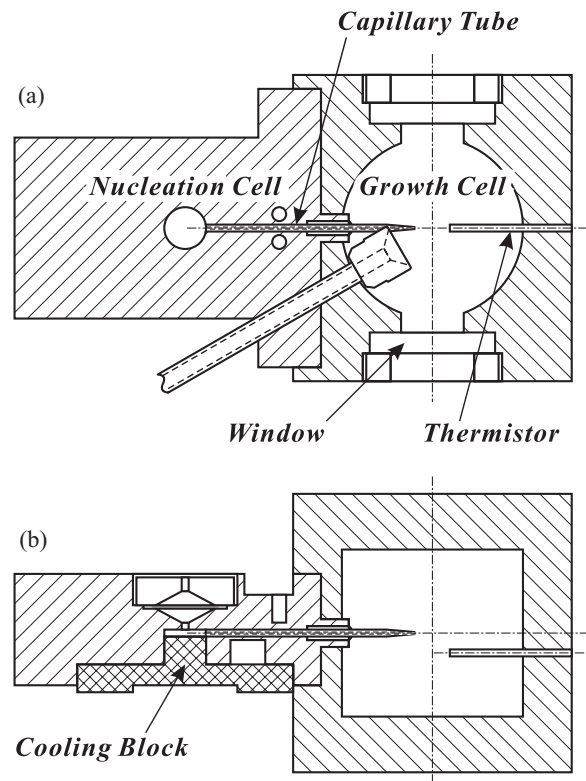


FIG. 3. Schematic view of the small experimental ice cell equipment used for microgravity experiments: (a) top view and (b) side view. The cell mainly consists of two parts, namely, the nucleation cell and the growth cell. Grains nucleated at the nucleation cell grow and propagate inside the capillary tube. The selected grain grows in the growth cell.

was installed in the ICC, and 1.6×1.2 mm (four-times view) in (b) since the crystal was small due to its initial phase. Here, the ice crystal grew from right to left. A capillary tube was set at the mid-right position in the figure, within which the crystal propagated after nucleation so that one grain could be selected. A thermistor was set at the lower-left corner in Fig. 1(a) to measure the temperature of the bulk water as a reference for the interferometric temperature measurements.

The ICC has another observation device, namely, an interferometer with the same field of view of the microscope, while the SCOF also has observation devices, namely, two interferometers and one amplitude-modulation microscope. The SCOF data are recorded via two cameras with a field of view of 3.2×2.4 mm (two-times view) and four-times view as shown in Fig. 1(b).

In the experiment, the nucleation cell was rapidly cooled to a sufficiently low temperature at which the nucleation would surely occur, namely, up to 10 K below the melting point, while the growth cell was maintained at a certain supercooling level. After detection of the latent heat at the nucleation cell, the temperature of the nucleation cell was set higher, the same as that of the growth cell in many cases, to prevent temperature perturbation at the growth cell.

The ICM performs outstandingly, especially in terms of temperature stability, as mentioned in Sec. IV in more detail. The growth cell can maintain almost constant temperature in the bulk water due to its large heat capacity and Peltier devices. Unfortunately, ice crystals grow not only toward the bulk water but also on the surface of the capillary tube toward the growth cell wall. Once the ice crystal reaches the wall, the ice also begins to grow on the wall. When the whole wall is covered with ice, the supercooling is canceled out since the temperature of the ice surface becomes the melting point due to the release of latent heat, thus limiting the duration of the experiment. Although this duration depends on the initial supercooling setting, it may range from a few to several tens of minutes under small supercooling conditions.

Although the supercooling at the growth cell was set from 0.03 to 2 K in the experiment, stable growth was only observed in the cases of 0.03 and 0.04 K. All the crystals observed under conditions where $\Delta T_{\text{set}} \geq 0.06$ K were unstable. We focused on aspects such as small supercooling in this paper to understand the stabilization mechanisms. When the supercooling was set to 0.02 K, the crystal was melted back, which indicates that the actual supercooling is at least 0.02 K smaller than the setting values; for example, the setting of 0.03 K is actually about 0.01 K or less. The SCOF has sufficient relative accuracy, on the order of 1/100 K, but lacks sufficient absolute accuracy for 1/100 K.

III. STABLE GROWTH MODEL

The typical time evolution of crystal thickness and radial size is shown in Fig. 4, where $\Delta T_{\text{set}} = 0.04$ K. Here, the solid and dashed lines represent thickness and size, respectively. A snapshot from the side view is shown in the lower-right corner of this figure. The shape of the side surface (prism plane) gradually approached a flat shape with time from an initial concave shape toward the water. Since the equilibrium shape of the ice crystal is slightly convex toward the water,

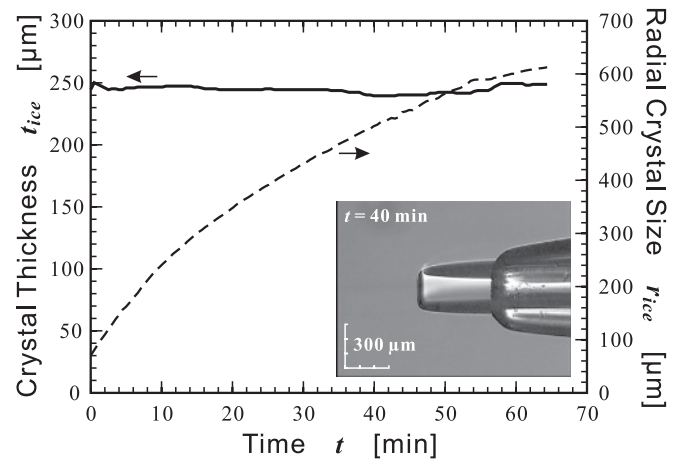


FIG. 4. Typical time evolution of crystal thickness and radial size. The supercooling is set to 0.04 K and a snapshot from the side view is shown in the lower-right corner in this figure. The solid and dashed lines represent crystal thickness and radial size, respectively. It is found that the thickness is almost constant, while the size increases over time.

the crystal approaches the near-equilibrium state as time progresses. This may be the essential reason why the radial growth rate decreases with time. To express this phenomenon, an adhesive growth model should be applied though a kinetic coefficient of the side surface but since this coefficient is unknown the model cannot be solved quantitatively. From a macroscopic point of view, however, the adhesive growth model may be replaced with macroscopic heat and mass balance models. Since the ice crystal is grown from the pure melt, the mass balance can be neglected.

From Fig. 4, the thickness is almost constant, 245 ± 2.5 μm , throughout the growth period. This indicates that the spiral growth rate or the frequency of the two-dimensional nucleation on the flat surface (basal plane) is negligibly small. Since the spiral growth stops at very low supercooling, the supercooling settings of 0.03 and 0.04 K should correspond to such low supercooling in our experiments. In addition, it is also indicated that the step on the flat surface advances with a very similar rate to the radial growth rate in those supercooling settings. Such the step advance can occur due to no supercooling threshold of the advance. This also suggests that the basal plane may not have an important role in the morphological instability.

By considering all of these phenomena, we may be able to estimate some important parameters such as the free energy of the step, the kinetic coefficient of the step advance, and so on in future, but these are not the topics of this paper. No observation of the thickness increase also means that the angle of the vicinal surface decreases with time. This may suggest another interesting issue of the change of the step intervals on the basal plane and related kink site density but these topics are also for future work. Based on the almost constant thickness, we do not consider thickness increase, that is, perpendicular growth to the basal plane, in this paper.

Thus the governing equations taken into consideration include thermal diffusion in the melt and the crystal and the balance of heat flux at interfaces. In two-dimensional r - z

coordinates, these are expressed as

$$\rho_i C_{p_i} \frac{\partial T}{\partial t} = \kappa_i \left(\frac{\partial^2 T}{\partial r^2} + \frac{1}{r} \frac{\partial T}{\partial r} + \frac{\partial^2 T}{\partial z^2} \right), \quad (1)$$

$$L_{SL} \rho \frac{\partial f}{\partial t} = -\kappa_L \left(\frac{\partial T}{\partial r} - \frac{\partial T}{\partial z} \frac{\partial f}{\partial z} \right)_L + \kappa_S \left(\frac{\partial T}{\partial r} - \frac{\partial T}{\partial z} \frac{\partial f}{\partial z} \right)_S, \quad (2)$$

$$-\kappa_L \left(\frac{\partial T}{\partial z} \right)_L + \kappa_S \left(\frac{\partial T}{\partial z} \right)_S = 0, \quad (3)$$

where ρ , κ , and L_{SL} represent the density, thermal conductivity, and latent heat, respectively. The suffix i takes s or L , which means solid or liquid regions. f is a function of z and t , which expresses the r coordinate of the interface shape of the side surface (prism plane), $r = f(z, t)$. Thus the radial growth rate is expressed as $\partial f / \partial t$. In Eq. (2), if L_{SL} takes the latent heat of solidification, ρ takes the liquid density.

To solve these equations simultaneously, the boundary-fitted coordinate (BFC) method [16,17] is used in this paper. In this method, the actual coordinates r - z are transformed to the computational coordinates ξ - η . The BFC method features automatic grid generation by solving the following equations:

$$\alpha r_{\xi\xi} - 2\beta r_{\xi\eta} + \gamma r_{\eta\eta} = 0, \quad (4)$$

$$\alpha z_{\xi\xi} - 2\beta z_{\xi\eta} + \gamma z_{\eta\eta} = 0, \quad (5)$$

where $\alpha = r_\eta^2 + z_\eta^2$, $\beta = r_\xi r_\eta + z_\xi z_\eta$, $\gamma = r_\xi^2 + z_\xi^2$, and J is the Jacobian, $J = r_\xi z_\eta - r_\eta z_\xi$. The suffixes ξ and η represent the partial differentials by ξ and η , respectively.

In the computational space, Eqs. (1)–(3) are transformed to

$$\begin{aligned} \rho C_p \left[\frac{\partial T}{\partial t} - \frac{1}{J} (z_\eta T_\xi - z_\xi T_\eta) - \frac{1}{J} (-r_\eta T_\xi + r_\xi T_\eta) \right] \\ = \kappa \frac{1}{J^2} (\alpha T_{\xi\xi} - 2\beta T_{\xi\eta} + \gamma T_{\eta\eta}) + \kappa \frac{1}{r} \frac{1}{J} (z_\eta T_\xi - z_\xi T_\eta), \end{aligned} \quad (6)$$

$$\begin{aligned} L_{SL} \rho \frac{\partial f}{\partial t} = -\kappa_L \frac{1}{J_L} \frac{1}{z_\eta} (\alpha T_\xi - \beta T_\eta)_L \\ + \kappa_S \frac{1}{J_S} \frac{1}{z_\eta} (\alpha T_\xi - \beta T_\eta)_S, \end{aligned} \quad (7)$$

$$\frac{1}{J_L} \kappa_L (-\beta T_\xi + \gamma T_\eta)_L = \frac{1}{J_S} \kappa_S (-\beta T_\xi + \gamma T_\eta)_S, \quad (8)$$

where the suffix i is eliminated in Eq. (6) to simplify the expression. In the model, the supercooling on the side surface (prism plane) is not considered, while that on the flat surfaces (basal plane) is considered. By solving Eqs. (6)–(8) simultaneously by using thermophysical properties shown in Table I, we found that there were no stable solutions, even though the supercooling of the bulk water was set to less than 0.01 K. The instability is mainly due to the the same mechanism as the Berg effect [18–20] at the edge of the crystal; hence the Gibbs-Thomson effect is considered to be a stabilization mechanism and is described as

$$T_m' = T_m - \frac{T_m}{l_{sl}} \left(\frac{\tilde{\alpha}_1}{R_1} + \frac{\tilde{\alpha}_2}{R_2} \right), \quad (9)$$

where T_m , T_m' , and l_{sl} represent the melting point, a varied melting point by the Gibbs-Thomson effect, and the latent

TABLE I. Summary of the thermophysical properties of ice and heavy water, which were used for the numerical simulation.

Properties		Solid	Liquid
Thermal Conductivity	[W/(m K)]	2.2	0.561
Density	[kg/m ³]	1.0177 × 10 ³	1.1056 × 10 ³
Specific Heat	[J/(kg K)]	2100	4217
Latent Heat	[J/kg]	3.36 × 10 ⁵	
Melting Point	[°C]	3.82	

heat per unit volume, respectively. R_i and $\tilde{\alpha}_i$ ($i = 1, 2$) are the principal radii and stiffness. The principal radius is described by using a function expressing the geodesic line g as

$$R = \frac{(1 + g'^2)^{3/2}}{|g''|}, \quad (10)$$

where the prime and double prime represent the first- and second-order differentials, respectively. The stiffness is described as

$$\tilde{\alpha}_i = \sigma(y) + \frac{\partial^2 \sigma}{\partial \theta_i^2}, \quad (11)$$

where $y = \tan \theta_i$, with θ_i and σ the angle between the normal and datum lines and the interfacial tension, respectively. Equation (10) is also transformed to computational coordinates as

$$R = \frac{(r_\eta^2 + z_\eta^2)^{3/2}}{|r_\eta z_{\eta\eta} - r_{\eta\eta} z_\eta|}. \quad (12)$$

In this paper, we assume the dependency of the interfacial tension on the angle to be negligibly small, and thus we obtain

$$\tilde{\alpha}_1 = \tilde{\alpha}_2 = \sigma_0, \quad (13)$$

where σ_0 is the interfacial tension of the {1010} plane.

To calculate the Gibbs-Thomson effect, the radii are required. It is easy to obtain one radius from the experiments, namely, the crystal radius. The other one, however, cannot be obtained from the experiments since it is difficult to obtain sufficiently magnified data near the edge. Therefore, we assume that the curvature of the side interface has a symmetric profile with respect to the interface of the flat surface at the edge, as shown in Fig. 5; Fig. 5(a) shows the whole crystal shape and Fig. 5(b) shows the magnified shape near the edge within the dashed circle in Fig. 5(a). The principal radius is calculated under this assumption and is often of the order of several tens of micrometers at the edge in many cases in this research, as shown in Fig. 5(c), though it depends on the crystal thickness and the supercooling. In Fig. 5(c), the dashed and solid lines represent the crystal shape and the arcs with the calculated principal radii, respectively. This method should bring us the largest principal radius at the edge and thus we can prevent overestimation of the Gibbs-Thomson effect. This approach is also regarded as the Mullins-Sekerka model applied not to the azimuthal direction but to the thickness direction.

Figure 6 shows the typical comparison between the calculation result and the experimental one under microgravity. Figure 6(a) is the comparison of the interface shapes. The calculation result is the same as Fig. 5(c). From Fig. 6(a), the

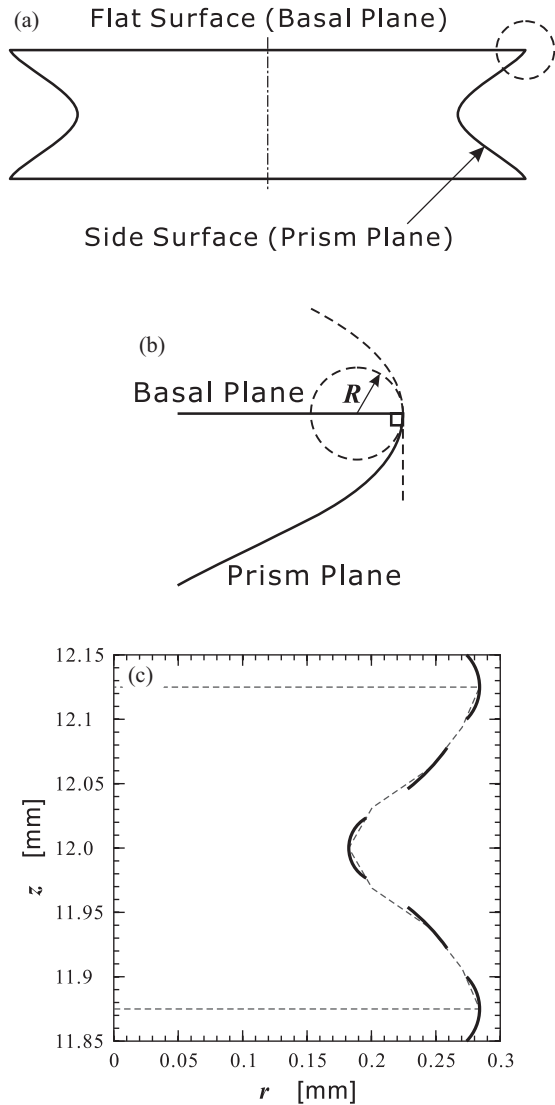


FIG. 5. Schematics of the crystal shape at the edge: (a) whole crystal shape and (b) magnified shape near the edge within the dashed circle in (a). The line of the side interface line is assumed to be virtually symmetric with respect to that of the flat surface. (c) An example of the principal radius calculation. The dashed and solid lines represent the ice boundary and arcs having radius of the principal radius, respectively. The principal radius at the edge is of the order of several micrometers.

difference between the calculation and experimental results seems to be of the order of $100 \mu\text{m}$. This difference should be caused by the large modeling region as compared with the crystal size, that is, 26 mm in diameter and 24 mm in height in this paper. This means that the coordinate error is around 0.5%. To improve this, increasing the number of the grids may be effective but this means a much longer CPU time. The most important point in this calculation is the degree of the Gibbs-Thomson effect. This is dominated by the principal radius and thus the comparison between the calculated principal radius and the experiment is shown in Fig. 6(b). The calculated radius is very similar to that of the experiment. This means that the degree of the Gibbs-Thomson effect is taken into account correctly.

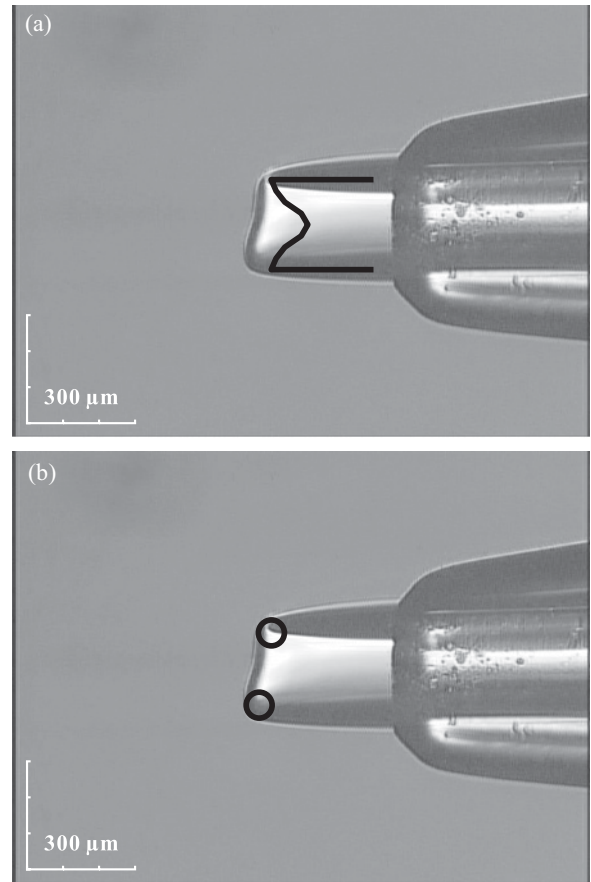


FIG. 6. Typical comparison results between calculation and experiments: (a) a comparison of the interface shapes on the side surface and (b) the principal radius obtained from the calculation. From (a), it is found that the shape difference between the calculation and the experiment is of the order of $100 \mu\text{m}$ at maximum. This should be caused by the large modeling region, that is, 26 mm in diameter and 24 mm in height. From (b), however, it is found that the principal radius is very similar to that of the experiment.

One example of the generated grids and a snapshot of the temperature distribution is shown in Fig. 7. Here, all regions of the growth cells were modeled since the reliable fixed boundary condition was the growth cell wall made of copper blocks. In Fig. 7(a), the region where dense vertical and horizontal grids crisscross each other corresponds to ice crystal. In Fig. 7(b), the bold solid line represents the shape of the ice crystal, while the thin solid and dashed lines are the isotherms. The temperature difference between the isotherms is $5/1000 \text{ K}$ in this figure. It is found that one dashed line crosses the flat interfaces, which indicates that the basal planes are supercooled. Although another solid line also crosses the side interface, this does not mean supercooling but is caused by the Gibbs-Thomson effect, and the temperature on the this plane always remains the same as the melting point.

IV. RESULTS AND DISCUSSION

To solve this model, although interfacial tension is required, it is unfortunately reported as wide-ranging from 15 to

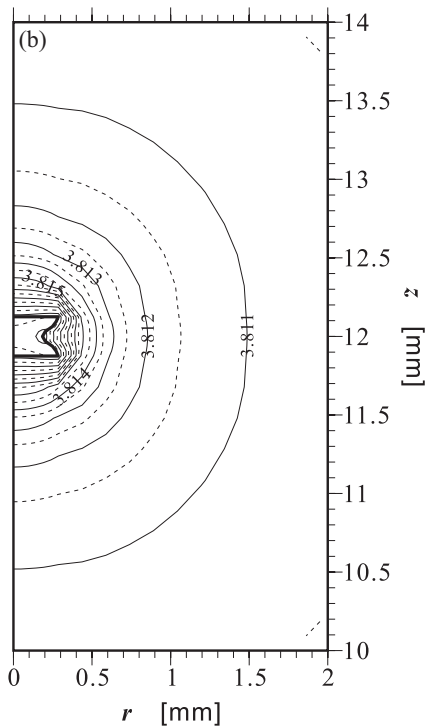
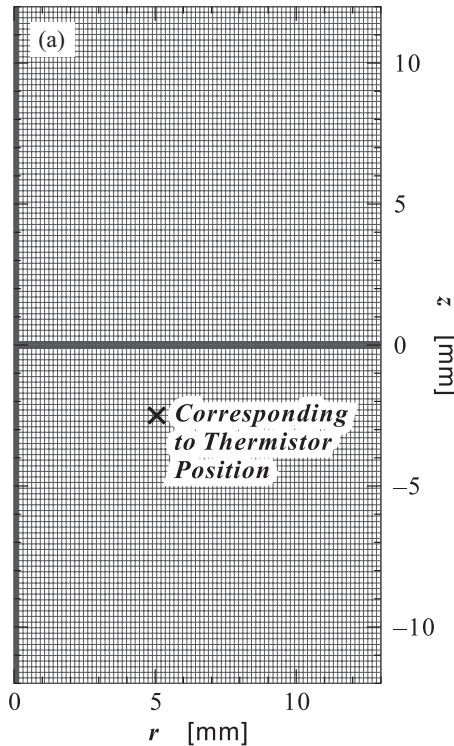


FIG. 7. Examples of (a) generated grids and (b) temperature distribution in the area magnified around the ice crystal. The cross in (a) represents the grid point corresponding to the thermistor set inside the water. All regions of the growth cell, 26 mm in diameter and 24 mm in height, are modeled. In (b), the bold solid line represents the shape of the ice crystal, while the thin solid and dashed lines represent the isotherms.

33 mJ/m² as mentioned in Sec. I. Since the wide variation is unsuitable for this work, the interfacial tension is estimated by

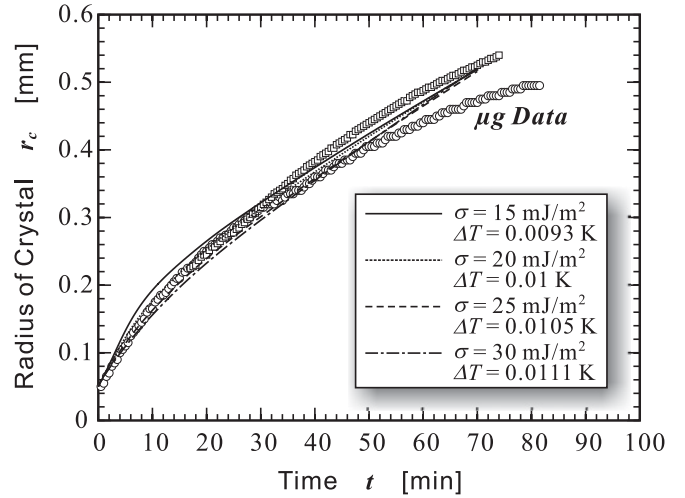


FIG. 8. A comparison of the time evolution of the crystal size between the calculation and experimental data under microgravity to estimate the interfacial tension. Although there are more microgravity data, the most reliable two data sets are selected as the reference. The surface tension is varied from 15 to 30 mJ/m² and the supercooling is also varied so that the final size is almost the same.

comparing the calculation results with the experimental ones under microgravity. The comparison result is shown in Fig. 8. Open circles and open squares represent the most reliable data under microgravity, which means that the influence of the ice growth on the cell wall is minimal. There are four kinds of lines in this figure; the solid, dotted, dashed, and dot-dashed lines represent the combinations of the tension of 15, 20, 25, and 30 mJ/m² and the supercooling of 0.0093, 0.01, 0.0105 and 0.0111 K, respectively. Larger tension needs larger supercooling due to the larger Gibbs-Thomson effect. The crystal thickness of 250 μm is used in this calculation as mentioned previously. The experimental results shown in Fig. 8 were obtained for $\Delta T_{\text{set}} = 0.03$ K, while the supercooling in the calculation is around 0.01 K by considering a supercooling shift of 0.02 K or more. This means that the supercooling of the calculation must be less than or equal to 0.01 K. The surface tension satisfying this criterion is in the range from 15 to 20 mJ/m². By careful comparison of the 15 mJ/m² case with the 20 mJ/m² case, it is found that the 20 mJ/m² case is better at explaining the experimental result in the initial time period within 20 min. Thus the interfacial tension of 20 mJ/m² is used in this paper.

Calculation data near the thermistor, which is shown in Fig. 3, are compared with measurement data as shown in Fig. 9 to investigate the reliability of the simulation. The bulk water temperature as measured by the thermistor is shown in Fig. 9(a). The measured data have noise of about ± 0.01 K. Since it is slightly difficult to determine the time trend, the noise is reduced by averaging the data points. The averaged data are shown in Fig. 9(b) as thin lines. There are two thin lines in this figure. One is for the data with $\Delta T_{\text{set}} = 0.03$ K and the other is for those with $\Delta T_{\text{set}} = 0.04$ K. It is found that the temperature remains almost constant during the experiment in the 0.03 K case, while it gradually increases over time in the 0.04 K case. The bold solid and dashed lines represent the calculation data in the cases of $\Delta T_{\text{sim}} = 0.01$ and 0.018 K,

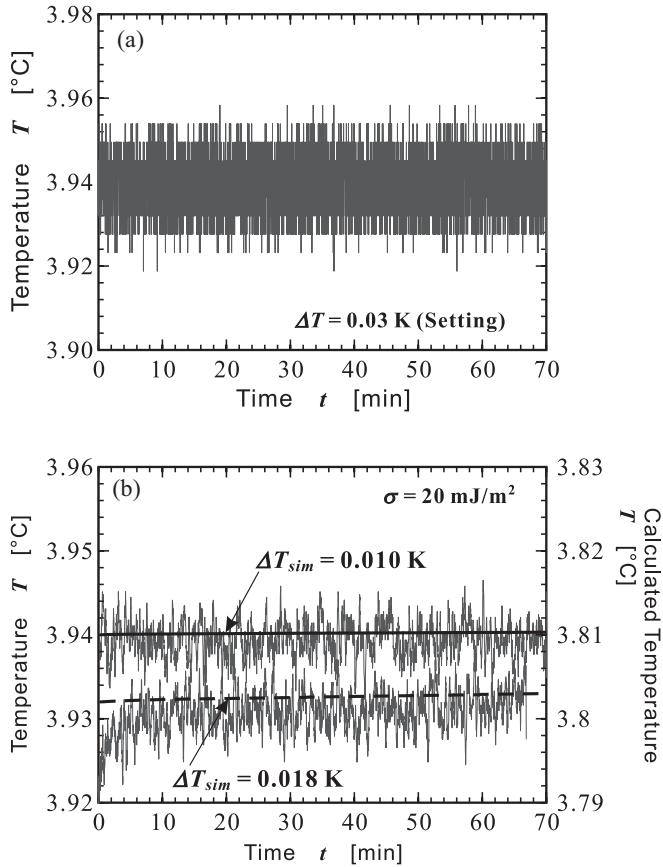


FIG. 9. Temperature comparison between calculation and experiments: (a) raw measurement data for $\Delta T_{\text{set}} = 0.03$ K and (b) comparisons in two cases of 0.03 and 0.04 K settings. In (b), thin lines and bold solid and dashed lines represent measurement and calculation data, respectively. ΔT_{sim} in (b) shows the supercooling, which is used in the computation. $\Delta T_{\text{sim}} = 0.01$ and 0.018 K correspond to $\Delta T_{\text{set}} = 0.03$ and 0.04 K, respectively.

respectively. This figure clearly shows that the calculation effectively explains the measured temperature, including the time trend.

By fixing the interfacial tension at 20 mJ/m^2 and varying the supercooling parameter of the simulation, the actual supercooling can be estimated. First, we change the supercooling parameter from 0.008 to 0.01 K to estimate the supercooling for $\Delta T_{\text{set}} = 0.03$ K. Subsequently, the parameter is changed from 0.016 to 0.02 K for the 0.04 K case. The comparison results are shown in Fig. 10. It is found that the simulation results agree well with the experimental ones until about 35 to 50 min in (a) and 20 to 30 min in (b). After those time periods, the crystal in the experiments grows more slowly than in the simulation or almost stops growing in some data. As mentioned in Sec. II, these slowdowns are caused by the ice growth on the cell wall. Therefore, the comparison is inadequate in the regions of (a) from 50 min to the end and (b) from 30 min to the end.

From Fig. 10, the actual supercooling for $\Delta T_{\text{set}} = 0.03$ K is estimated as $\Delta T = 0.009 \pm 0.001$ K and that in the 0.04 K case is $\Delta T = 0.018 \pm 0.002$ K, which means that the temperature in the growth cell is controlled with high precision, on the order of $1/100$ K. From this estimation, the temperature shift

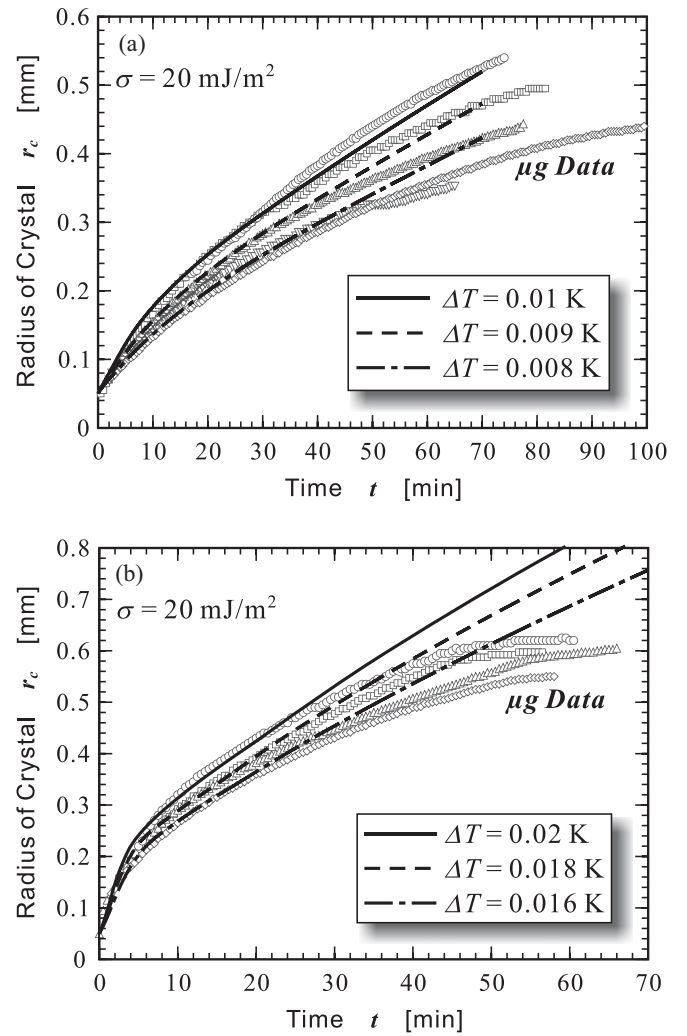


FIG. 10. Comparison of time evolution of crystal size between simulations by varying the supercooling conditions and experimental results: (a) $\Delta T_{\text{set}} = 0.03$ K and (b) $\Delta T_{\text{set}} = 0.04$ K. Points such as open circles represent the experimental results. Solid, dashed, and dot-dashed lines represent the numerical results in the cases of $\Delta T_{\text{sim}} = 0.01$, 0.009 , and 0.008 K, respectively, in (a), while those represent the results in $\Delta T_{\text{sim}} = 0.02$, 0.018 , and 0.016 K in (b).

between the setting and actual temperature should be 0.021 to 0.022 K, which is consistent with initial expectations. In Fig. 10, the experimental data seem to be scattered by several tens of percent. From the supercooling estimation, it is found that this scattering is caused by temperature variation on the order of $1/1000$ K, which is out of the ICM performance range.

Since our model is applicable to stable growth, the calculation will diverge in the event of instability. Therefore, the supercooling limit for stable growth is investigated by changing the supercooling parameter. For a crystal thickness of $250 \mu\text{m}$, it is found that the supercooling of 0.023 K is stable but that of 0.024 K is unstable, as shown in Fig. 11. The bold solid and dot-dashed lines represent the numerical results in $\Delta T_{\text{sim}} = 0.023$ K and 0.024 K cases, respectively, while the thin dashed line is the result in the 0.02 K case, which is the same as that shown in Fig. 10(b). In the 0.024 K

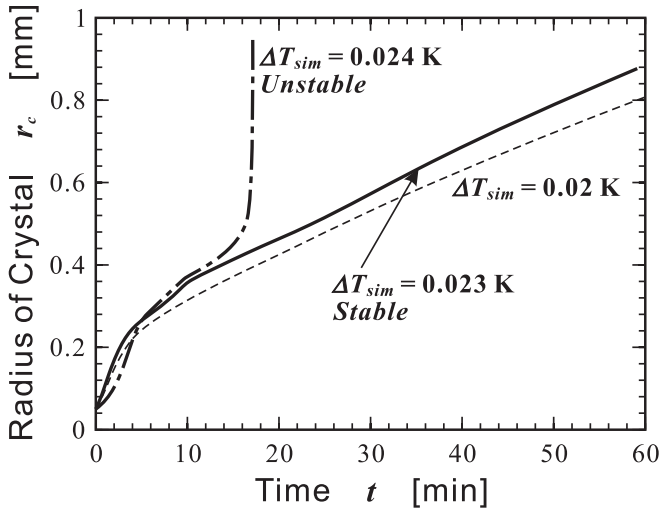


FIG. 11. Simulation results to investigate the stability limit. Thin dashed, bold solid, and bold dot-dashed lines represent the results for $\Delta T_{sim} = 0.02$ K for reference, 0.023 K, and 0.024 K. In the latter case, the crystal size grows rapidly at about 15 min, whereupon the calculation diverges.

case, the crystal size rapidly increases after about 15 min, whereupon the calculation diverges. Since the rapid increase in size means a large growth rate, the crystal morphology should be transformed to dendrites, meaning the supercooling limit may be 0.023 K. The temperature difference between the calculation and experimental results is 0.021 to 0.022 K as mentioned previously. Hence, $\Delta T_{sim} = 0.023$ K corresponds to $\Delta T_{set} = 0.045$ K, which is consistent with the experimental result. If the supercooling is just set to 0.045 K and the crystal thickness is 250 μm , the morphological transition may be observed but equipment capable of controlling the temperature on the order of 1/1000 K is required. We obtained some data in the 0.05 K setting but the crystal thickness was thinner than 250 μm . The typical result is shown in Fig. 12. Here, the crystal edge seems to undulate but a longer observation

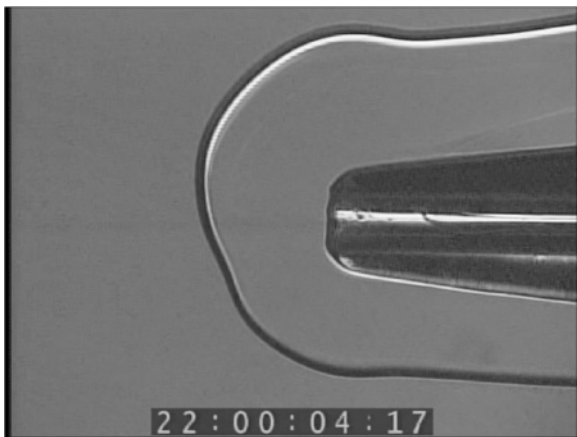


FIG. 12. Typical observation data in the $\Delta T_{set} = 0.05$ K case. The thickness is about 170 μm . The transition may occur if the observation period is sufficient.

period is required to clarify whether or not the transition can be observed under microgravity.

The supercooling limit should fluctuate if the crystal thickness varies, since the Gibbs-Thomson effect varies. This suggests that a certain limit of the crystal thickness may exist at a certain supercooling. This limit is called the critical thickness [3,9]. The supercooling limit in a wider range of the thicknesses will be investigated based on our model in the near future.

No morphological transition was observed under microgravity. Conversely, this transition is usually observed on the ground. This suggests that the instability is strongly affected by thermal convection, which causes the temperature nonuniformity. Nonuniformity of as little as 1/100 K may be sufficient to cause such instability, based on our study in this paper.

V. CONCLUSIONS

From December 2008 to February 2009, we carried out microgravity experiments of ice crystal growth in heavy water. We obtained more than 130 sets of data successfully. However, despite our initial expectation, the morphological transition, which was the key target in the microgravity experiments, was not observed. To understand why stable growth was maintained throughout the experiment under small supercooling conditions, a two-dimensional model was introduced. In order to explain the experimental data, this model required a stabilization mechanism, and hence the Gibbs-Thomson effect was included in the model. To calculate the Gibbs-Thomson effect, interfacial tension was required. We estimated the tension by comparing the numerical results with the experimental ones. After comparison, we decided to use a tension of 20 mJ/m^2 . It is also found that the numerical results agreed well with the time evolution of temperature near the crystal in the bulk water, which indicates the reliability of the model.

In addition, the actual supercooling is estimated because the supercooling setting was shifted from the actual supercooling, with a suggested difference of about 0.02 K from the experiments. The simulation showed a difference of 0.021 to 0.022 K. It is also found that the SCOF has excellent performance in terms of relative temperature control, on the order of 1/100 K.

The instability trigger may be the temperature fluctuation caused by the thermal convection on the ground. Small fluctuations of the order of the 1/100 K may be enough to work as a trigger of the instability. The microgravity environment is suitable for such a sensitive experiment since thermal convection can be suppressed sufficiently.

ACKNOWLEDGMENTS

The ICM was mainly developed by Mr. T. Tomobe at IHI Aerospace Co., Ltd., through his great efforts. The authors appreciate him deeply. We are also thankful to Mr. T. Sone at the Japan Manned Space Systems Corporation for his dedicated efforts in ground-based facility tests and operations of the microgravity experiments.

- [1] K. Arakawa and K. Higuchi, *J. Faculty Sci.* **4**, 201 (1952).
- [2] K. Arakawa, *J. Glaciol.* **2**, 467 (1955).
- [3] Y. Furukawa and E. Yokoyama, in *Proceedings of the First International Symposium on Microgravity Research and Applications in Physical Sciences and Biotechnology*, edited by B. Schürmann, ESA-SP-454 (European Space Agency, Noordwijk, 2001), p. 465.
- [4] Y. Furukawa, E. Yokoyama, and W. Shimada, in *Studies on Crystal Growth under Microgravity*, edited by Y. Hayakawa and Y. Furukawa (Research Signpost, Trivandrum, India, 2005), p. 165.
- [5] T. Fujioka and R. F. Sekerka, *J. Cryst. Growth* **24/25**, 84 (1974).
- [6] T. Kuroda and R. Lacmann, *J. Cryst. Growth* **56**, 189 (1982).
- [7] T. Kuroda, in *Morphology and Growth Unit of Crystals*, edited by I. Sunagawa (Terra Scientific Publishing Company (TERRAPUB), Tokyo, 1989), p. 577.
- [8] E. Yokoyama, R. F. Sekerka, and Y. Furukawa, *J. Phys. Chem. B* **104**, 65 (2000).
- [9] W. Shimada and Y. Furukawa, *J. Phys. Chem. B* **101**, 6171 (1997).
- [10] E. Yokoyama, R. F. Sekerka, and Y. Furukawa, *J. Phys. Chem. B* **113**, 4733 (2009).
- [11] S. Adachi *et al.*, *J. Jpn. Soc. Microgravity Appl.* **18**, 228 (2001) (in Japanese).
- [12] Y. Furukawa *et al.*, in Proc. 26th Symp. Space Utilization Res., Kanagawa, Japan, 2010 (unpublished).
- [13] E. Yokoyama *et al.*, *J. Phys. Chem. B* **115**, 8739 (2011).
- [14] S. C. Hardy, *Philos. Mag.* **35**, 471 (1977).
- [15] W. M. Katcham and P. V. Hobbs, *Philos. Mag.* **19**, 1161 (1968).
- [16] J. F. Thompson, F. C. Thames, and C. W. Mastin, *J. Comput. Phys.* **15**, 299 (1974).
- [17] K. Fujii, in *Numerical Methods for Computational Fluid Dynamics*, Chap. 7 (University of Tokyo Press, Tokyo, 1994) (in Japanese).
- [18] W. F. Berg, *Proc. R. Soc. London Ser. A* **164**, 38 (1938).
- [19] C. W. Bunn, *Discuss. Faraday Soc.* **5**, 132 (1949).
- [20] T. Kuroda, T. Irisawa, and A. Ookawa, *J. Cryst. Growth* **42**, 41 (1977).